Advanced Power Management Technology for High-Voltage High-Power Batteries

Thomas H. Sobota, Yiming Lou, and Michael A. Johnson
Advanced Projects Research, Inc.
1925 McKinley Ave. Suite B, La Verne, CA, 91750

Abstract: *This paper describes advanced cell-level monitoring and control algorithms and their application for battery power management. The battery power management system developed by APRI has the capability to estimate cell state of charge (SoC) and internal resistance indicative of state of health (SoH); and to control the SoC of each individual cell in high-voltage, high power battery packs. The designed battery power management system has been tested on a 24-cell lithium-ion battery pack using hardware designed and manufactured by APRI. Test results show that the cell-level estimator can accurately estimate the evolution of cell SoC and can effectively capture the variation of battery internal resistance due to the aging effect to indicate battery SoH; and feedback control can significantly reduce pack imbalance and increase the effective pack capacity.*

Keywords: Cell-Level Control; Monitoring; SoC; SoH; Lithium Ion.

Introduction

This research is motivated by the recognized need for monitoring and controlling battery function at the cell level. Today's high power semiconductor technology permits high battery voltages. These voltages require series strings of many cells depending on the electrochemical couple selected. Repeated discharges of these long series strings of cells, especially deep discharges, may cause a battery to become unbalanced, which will lead to accelerated degradation and eventually premature failure [1]. Because of the cell to cell variability in performance and the interactions between cells described above, it is desirable to monitor the performance of a battery energy storage system on a cell by cell basis. The ability to do so can be used to prolong battery life as well as reliability and safety.

In this work, we aim at the development of a systematic framework for the design of a power management system that integrates real-time current/voltage measurements, cell-level mathematical models, and feedback control algorithms to regulate the SoC of individual cell in a high-voltage, high-power battery pack in real time. One of the main obstacles for real-time feedback control is the difficulty to obtain real-time measurements of cell SoC without interrupting normal battery operations. We design and experimentally implement a model-based battery SoC and SoH estimator using the extended Kalman filtering technique [2,3]. The real-time SoC and SoH estimator enables the design of a feedback controller to regulate the SoC of each individual cell in a high-voltage, high-power battery pack. The control problem is formulated as the one that regulating the SoC of each individual cells in a multiple-cell battery pack by manipulating the shunt current through the shunt resistor associated to each cell. A control system is designed that couples the cell estimator to a model-based controller so that the SoC estimates obtained from the cell SoC and SoH estimator are used by the controller to determine the appropriate amount of shunt current to reduce the battery imbalance. Finally, a battery test is carried out to implement the designed energy management system to a 24-cell Lithium-Ion battery pack for demonstration. Significant reduction of pack imbalance and increase of effective pack capacity are observed in the test.

Cell-Level SoC and SoH Estimator Design

For cell performance monitoring, cell SoC and SoH are two most important variables that indicate the condition of a cell. SoC measures the ratio of how much charge is left in the cell to the cell total capacity and SoH is used to indicate how well the cell is functioning relative to its nominal states, which is often represented by cell resistance and capacity [4]. Having access to SoC and SoH of each individual cells in real-time is essential for per-cell monitoring and control.

In this section, we design a cell-level SoC and SoH estimator using a cell-level model and an advanced nonlinear state and parameter estimation algorithm. An equivalent-circuit cell-level model is used as a basis for the estimator design and the extended Kalman filter (EKF) [5], a nonlinear extension of the Kalman filter, is adopted as the estimation algorithm.

A Cell-Level Model

We consider a cell-level model taking the following discrete-time form:

$$\begin{aligned} \begin{bmatrix} i_{2,k+1} \\ z_{k+1} \end{bmatrix} &= \begin{bmatrix} \alpha & 0 \\ 0 & 1 \end{bmatrix} \begin{bmatrix} i_{2,k} \\ z_k \end{bmatrix} + \begin{bmatrix} 1-\alpha \\ \frac{\eta}{C_n} \end{bmatrix} I_k + \begin{bmatrix} \omega_{1,k} \\ \omega_{2,k} \end{bmatrix} \\ y_k &= OCV(z_k) + I_k R_1 + i_{2,k} R_2 + \nu_k \end{aligned} \tag{1}$$

where z is the SoC, α is the time constant, R_1, and R_2 are resistors, i_2 is the current through R_2, I is the overall charging/discharging current, C_n is the capacitance, η is the cell coulombic efficiency, ω_1 and ω_2 are unmeasured process noises, ν_k is measurement noise and y_k is the cell

terminal voltage measurement. The OCV(z) is the correlation between the cell open-circuit-voltage and the cell SoC, which can be obtained from the battery manufacturer. R_1 represents the lumped series resistances for the solid and liquid phases and R_2 represents the lumped interfacial resistances. The equivalent circuit used to derive the model can be found in [6].

The Extended Kalman Filter

The extended Kalman filter is a predictor-corrector type estimation algorithm to estimate the parameters and states of a nonlinear system. We consider the general form of the mathematical model of a nonlinear system as follows:

$$\begin{aligned} \theta_{k+1} &= \theta_k + \zeta_k \\ x_{k+1} &= f(x_k, \theta_k, i_k) + \omega_k \\ y_k &= h(x_k, \theta_k, i_k) + \nu_k \end{aligned} \tag{2}$$

where k is the time index, x_k is the model state vector, i_k is the process input, θ_k is the model parameters vector, y_k is the process output, ω_k is unmeasured process noise and v_k is measurement noise. Nonlinear functions f and h are the state transition function and the output function, respectively.

The operation of the extended Kalman filter includes two steps: linearization and standard Kalman filter. In the linearization step, at each time index, k, nonlinear functions, $f(x_k, \theta_k, i_k)$ and $h(x_k, \theta_k, i_k)$ are linearized by their first-order Taylor expansions. Based on the linearized system, the standard Kalman filter can be directly applied to estimate θ_k and x_k based on the nonlinear process model of (2). When the cell SoC is one of the states of the model and the cell internal resistance indicative to battery SoH is one of the parameters of the model, EKF can be used to estimate the SoC and SoH at cell-level in real-time. The details of the operation of an EKF are omitted in this paper due to space limitation. The readers may refer to [5] for mathematical description of the EKF for general nonlinear systems.

Feedback control design

The control objective is to balance the SoC of different cells in a battery pack. A charge bleed circuit is used to balance the state of charge of different cells in the battery pack. With charge bleed, power is selectively bled off of the stronger cells using a bypass resistor. Electronics on each cell's control board switch the bleed resistor into and out of contact with the cell, determining whether or not current is being drained from that cell. The time fraction that the bleed resistor is switched into the circuit is the bleed fraction. The effective bleed current is defined as the product of bleed fraction and the bleed current when the bleed resistor is switched into the cell. We formulate our control problem as the one that balancing the state of charge of different cells in the battery pack by manipulating the effective bleed current of each cell.

A feedback control algorithm is designed to compute the effective bleeding current as follows:

$$I_{bleed,i}(k) = \beta \cdot (\hat{z}_b(k) - \hat{z}_i(k)) \tag{3}$$

where $I_{bleed,i}(k)$ is the effective bleed current for cell i at time index k, $\hat{z}_b(k)$ is the estimated SoC of cell b, the weakest cell in the pack, $\hat{z}_i(k)$ is the SoC of cell i, and β is the controller gain, which governs the rate of convergence of the system under control and is designed based on the cell-levle model.

The estimated SoC for both cell b and cell i required by the feedback control algorithm of (3) are provided by the designed cell estimator. The controller of (3) is, therefore, coupled with the cell SoC and SoH estimator to form an estimator/controller structure to control the SoC of the battery pack at individual cell level. The estimator/controller structure is shown in Figure 1.

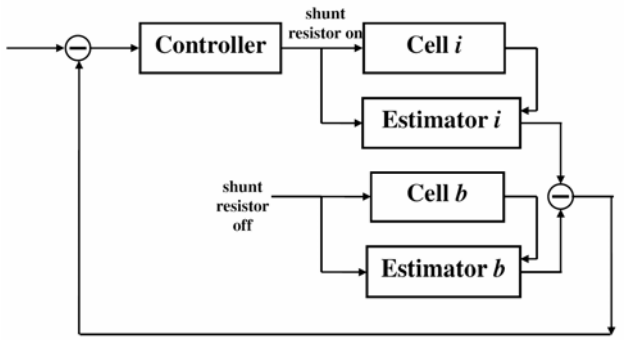

Figure 1. The estimator/controller structure

The structure shown in Figure 1 is very effective for the control of many complex processes where the quantities of the controlled variables cannot be directly measured in real-time and estimation techniques are required to acquire these quantities.

Test results

APRI built a battery pack around twenty-four GP18650 Lithium-ion cells, as shown in Figure 3, to test the developed cell-level monitoring and control algorithms. The cells are connected in 3 strings in parallel and each string contains 8 cells in series, giving us an overall voltage of more than 30V. In the test, current and voltage measurements are obtained by using an Agilent 34970A data acquisition unit. An Agilent 6653A DC power supply is used to charge the battery and an Agilent 6060B DC electronic load is used for discharging the battery. Repeated cycles of charge/discharge are used. Each cycle follows the constant current discharging, constant current charging and constant voltage charging pattern.

We first calibrate the cell-level model of (2) using a GP1865L200 Lithium Ion cell. $OCV(z)$ function is obtained by interpolating test data from the manufacture using the cubic spline interpolation technique. The model calibration

result is presented in Figure 2. The top plot shows the comparison of the cell terminal voltage profile predicted by the cell model of (1) (solid line) and that obtained from measurement (dotted line). The error of the two profiles is plotted in the bottom. It can be observed that the model error is very small in most of the time during the test. The high fidelity of the model makes it a good basis for model based monitoring and control system design.

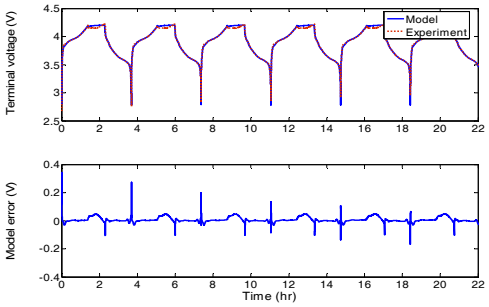

Figure 2: Result of Model Calibration

We tested the cell SoC and SoH estimator using cell current and terminal voltage data collected in a 35-day test. The test results obtained during the first day is presented in Figure 4. In the top plot of Figure 4, the solid line shows the estimated cell state of charge, and the dotted line shows the cell state of charge computed by using ampere hour counting, which is considered to be 'true' SoC of the cell. The bottom plot of Fig. shows the error between the SoC estimates and that obtained from ampere hour counting. It can be seen that the two profiles are very close and the estimation error is about 5%. Throughout the 35-day of the test, the high accuracy of the SoC estimate is maintained. The evolution of the cell internal resistance obtained by the SoC and SoH estimator during the 35-day test is shown in Figure 5. The resistance gradually increases from about 80mΩ to about 120mΩ due to the aging during the repeated cycling.

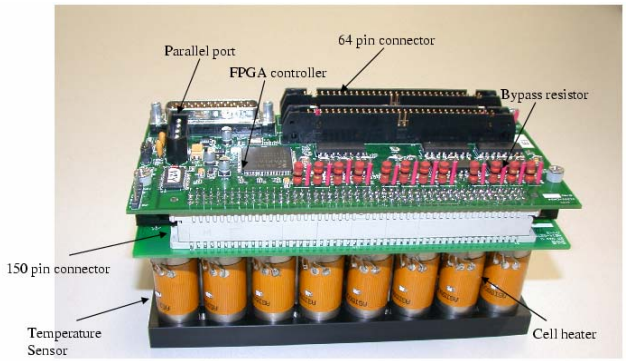

Figure 3. The 24-Cell Battery Pack with Controller Board

We tested the feedback control system to demonstrate the capability of the control system to effectively reduce pack level imbalance and increase of effective pack capacity. To do this, the 24-cell battery pack was initially unbalanced. Specifically, cells no. 6, 7, and 8 are much stronger than the rest of the cells in the pack. The initial values of SoC of these strong cells are about 20% higher. The test lasted for 10 cycles and the test results are presented in Figure 6 to Figure 10.

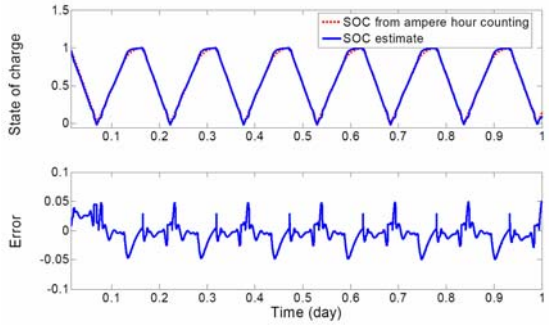

Figure 4: Test results of the SoC and SoH estimator

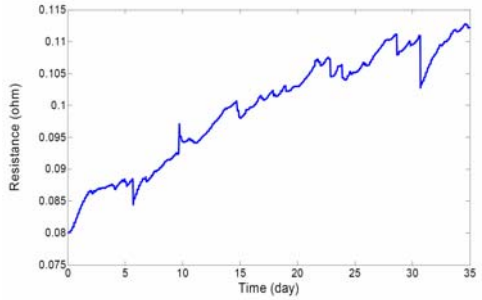

Figure 5: Evolution of the Internal Resistance from the SoC and SoH Estimator

Figure 6 shows the evolution of terminal voltage of each individual cell in the 24-cell battery pack under control. During the first cycle, two very different terminal voltage profiles are observed, one is high and one is low. The high voltage profile representing evolution of terminal voltages in the three strong cells (cells 6, 7, and 8) and the low voltage profile representing the evolution of terminal voltages in the rest of cells in the pack. It is seen that after 3 cycles, the difference between the two profiles is not as apparent as it is during the first cycle, which is a sign of improved balance of the battery pack due to the implementation of the controller. In Figure 7, the evolution of the estimated SoC of each cell in the battery pack is presented. Again, it is clear that after three cycles, the profiles of SoC of all cells in the pack are very close to each other.

To demonstrate the improved balance of the cells in the battery pack, a plot of the difference between the highest and lowest terminal voltages in the pack at the end of each constant voltage charge mode (when the pack is fully charged) is shown in Figure 8. This difference is about 0.19 V at the beginning of the test and is reduced to about 0.03V at the end of the test. Furthermore, starting at the 4th cycle, this difference is stabilized within 0.04V. In terms of the

SoC, the SoC difference between the strongest and weakest cells at the end of each cycle is plotted in Figure 9. Initially, there is a difference of 18% SoC between the strongest and the weakest cells in the pack, and this difference is reduced to around 3% by the designed controller. In summary, the designed estimator/controller structure successfully balances the SoC of battery cells in a 24-cell battery pack within 4 charge/discharge cycles.

There are many benefits of individual cell-level control to high-voltage, high-power batteries. Implementing the designed controller to the battery pack can significantly increase the useful capacity of the pack because the controller can significantly reduce the imbalance of a battery pack. Figure 10 shows the increase of discharge capacity of the battery pack. The discharge capacity is computed by counting the current flowing out of the battery pack from the fully charged state to the fully discharged state at constant discharge current of 2.4A. It can be observed that in the first cycle, due to the imbalance of the pack, only 34Ah can be discharged from the battery pack from its fully charged state to its fully discharged state. This capacity increases as the controller is working to balance the pack. In the second cycle, this capacity increases to above 38Ah. After 4 cycles, the discharge capacity of the pack is approximately 44Ah and stable at this value.

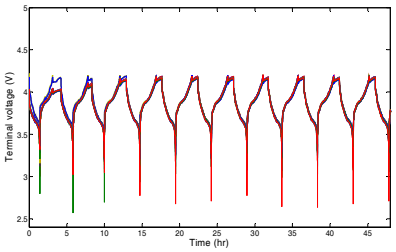

Figure 6: Profiles of the Terminal Voltage for the 24 Cells under Control

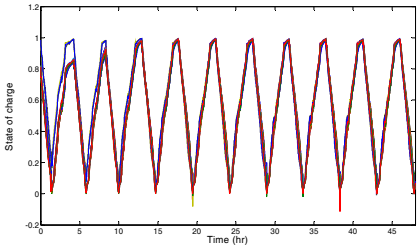

Figure 7: Profiles of the SoC of 24 Cells under Control

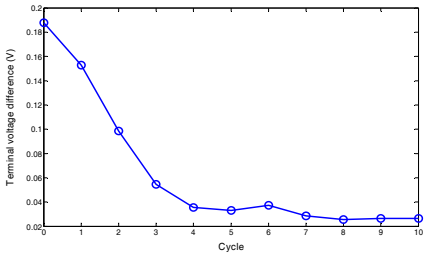

Figure 8: Difference of the Terminal Voltage at the End of Each Cycle

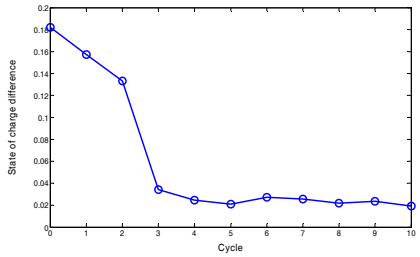

Figure 9: SoC Imbalance at the End of Each Cycle

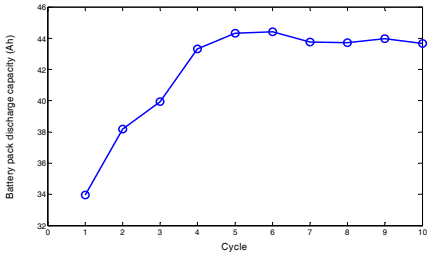

Figure 10: Increase of the Discharge Capacity of the Battery Pack Due to the Feedback Control

Acknowledgements

The authors are grateful for the financial support of the project by the U.S. Air Force under contract no. FA8650-04-D-2458.

References

1. Jossen, A., V. Spath, H. Doring, and J. Garche., "Reliable Battery Operation - A Challenge for the Battery Management System," *Journal of Power Sources*, 84:283–286, 1999.
2. Piller, S., M. Perrin, and A. Jossen. "Methods for State-of-Charge Determination and Their Applications," *Journal of Power Sources*, 96:113–120, 2001.
3. Plett, G. L., "Extended Kalman Filtering for Battery Management Systems of LiPB-Based HEV Battery Packs Part 2. Modeling and identification," *Journal of Power Sources*, 34:262–276, 2004.
4. Verbrugge, M., D. Frisch, and B. Koch., "Adaptive Energy Management of Electric and Hybrid Electric Vehicles," *Journal of the Electrochemical Society*, 152:A333–A342, 2005.

5. Wan, E. A., and A. T. Nelson, "Dual Extended Kalman Filter Methods," In *Kalman Filtering and Neural Networks* (Ed. S. Haykin), 123-174, John Wiley, New York, 2005.

6. Verbrugge, M. W., and R. S. Conell. "Electrochemical and Thermal Characterization of Battery Modules Commensurate with Electric Vehicle Integration," *Journal of the Electrochemical Society*, 149:A45–A53, 2002.